Dynamic capillary effects in a small-volume unsaturated porous medium: Implications of sensor response and gas pressure gradients for understanding system dependencies

Lili Hou,[1] Lixia Chen,[1] and Tohren C. G. Kibbey[1]

Received 22 May 2012; revised 21 September 2012; accepted 12 October 2012; published 16 November 2012.

[1] Rate dependencies in system properties observed during nonsteady state unsaturated and multiphase flow are often referred to as dynamic capillary effects. One widely studied dynamic capillary effect is the apparent dependence of measured capillary pressure on the rate of saturation change. While this phenomenon has been observed for over four decades, a clear picture of the source of the phenomenon and its true magnitude remains elusive. Furthermore, reported dependencies on system properties and state variables have been contradictory. The focus of this work was on quantifying the relationship between measured capillary pressure and rate of saturation change using a small volume system with highly characterized fluid-selective microsensors. Experimental measurements in three systems were used to calculate the dynamic capillary coefficient τ as a function of saturation during drainage. Corrections for sensor response and flow-induced gas pressure gradients were applied to explore how these potential artifacts would impact measured τ values. Significant differences in τ values were observed in uncorrected measurement between the three systems, but corrected values were very similar in all cases. Corrected τ values were found to be on the order of 10^3 Pa s or less—one to two orders of magnitude lower than the uncorrected values, and two or more orders of magnitude lower than most published values for similar porous medium/fluid combinations. Because of the small size of the experimental system used, results suggest that at the representative elementary volume (REV) scale, the dependence of measured capillary pressure on the rate of saturation change may not be as significant as previously thought for unsaturated systems. It is hypothesized that the larger magnitude of some previously reported τ values may result at least in part from porous medium packing microheterogeneities that influence flow and pressure gradients in larger systems.

Citation: Hou, L., L. Chen, and T. C. G. Kibbey (2012), Dynamic capillary effects in a small-volume unsaturated porous medium: Implications of sensor response and gas pressure gradients for understanding system dependencies, *Water Resour. Res.*, *48*, W11522, doi:10.1029/2012WR012434.

1. Introduction

[2] The nonsteady state movement of multiphase fluids in porous media plays a central role in problems involving a wide range of systems. Examples of problems where the dynamics of saturation change may be important include enhanced oil recovery, geologic carbon sequestration, migration and remediation of nonaqueous phase liquids (NAPLs) in the subsurface, and infiltration/flooding phenomena in extreme weather events. Accurate modeling of these systems requires a quantitative understanding of the dynamic relationships between fluids in porous media undergoing saturation change.

[3] The capillary pressure-saturation (P_c-S) relationship, also known as the soil water characteristic curve or the water retention function, is an important constitutive relationship governing multiphase flow [*Huyakorn and Pinder*, 1986; *Muraleetharan and Wei*, 1999]. Capillary pressure in a porous medium P_c is defined as the pressure in the nonwetting phase minus the pressure in the wetting phase. In problems of multiphase or unsaturated flow, the wetting phase is typically defined as the phase through which contact angle (the angle between the fluid-fluid interface and the solid surface) is less than 90 deg. In many natural porous media, water is the wetting phase, while air or organic liquid is the nonwetting phase. Wetting phase saturation S is the fraction of the pore volume occupied by the wetting phase. The P_c-S relationship describes the relationship between P_c and S in a medium. The relationship is hysteretic, in that the specific value of P_c at a given S depends on the wetting/drying path followed to reach that S.

[1]School of Civil Engineering and Environmental Science, University of Oklahoma, Norman, Oklahoma, USA.

Corresponding author: T. C. G. Kibbey, School of Civil Engineering and Environmental Science, University of Oklahoma, 202 W. Boyd St., Rm. 334, Norman, OK 73019, USA. (kibbey@ou.edu)

0043-1397/12/2012WR012434

[4] P_c-S relationships have historically been measured under static equilibrium conditions. Because of the dynamics of multiphase flow, particularly in fine porous media, it can take hours or even days for fluids to reach their equilibrium states during measurement steps. For this reason, experimental measurement of equilibrium P_c-S relationships can require weeks or months to complete for some fine-grained porous media [*Dane and Hopmans*, 2002]. More than four decades ago it was observed that when P_c-S relationships are measured more rapidly (i.e., where pressure is changed before equilibrium has been reached), the measured relationship differs from the static equilibrium P_c-S relationship [e.g., *Topp et al.*, 1967; *Smiles et al.*, 1971]. This phenomenon has come to be referred to as a dynamic capillary effect.

[5] Dynamic capillary effects refer to the observed flow rate dependence of fluid states in porous media experiencing dynamic drainage or imbibition. Besides capillary pressures, other phenomena that have been found to exhibit dynamic capillary effects include relative permeability [*Stauffer*, 1978; *Barenblatt et al.*, 2003], and the spatial distribution of fluids [*Wildenschild et al.*, 2005]. While it is probable that all of these observed phenomena are related, a comprehensive, quantitative understanding of dynamic capillary effects remains elusive. Dynamic capillary effects have been observed by a number of well-designed experiments and studied by many theoretical analyses and modeling simulation efforts, but to date the observed and predicted system dependencies have been largely contradictory [*Topp et al.*, 1967; *Stauffer*, 1978; *Wildenschild et al.*, 2001; *Manthey et al.*, 2005; *Oung et al.*, 2005; *Wildenschild et al.*, 2005; *Camps-Roach et al.*, 2010; *Sakaki et al.*, 2010; *Bottero et al.*, 2011; *Goel and O'Carroll*, 2011; *Das and Mirzaei*, 2012]. Proposed mechanisms of dynamic capillary effects have included dynamic contact angles [*Weitz et al.*, 1987; *Friedman*, 1999], dynamic interface deformation [*Weitz et al.*, 1987; *Kalaydjian*, 1992], dynamic fluid spatial distribution [*Wildenschild et al.*, 2001; *Barenblatt et al.*, 2003; *Wildenschild et al.*, 2005], and the effects of averaging homogeneous/heterogeneous flow zones [*Bourgeat and Panfilov*, 1998; *Dahle et al.*, 2005; *Gielen et al.*, 2005].

[6] Several quantitative relationships have been proposed to describe the effect of dynamic saturation change on capillary pressure [*Stauffer*, 1978; *Hassanizadeh and Gray*, 1990; *Kalaydjian*, 1992; *Hassanizadeh and Gray*, 1993b, 1993a; *Hassanizadeh et al.*, 2002; *Barenblatt et al.*, 2003]. Most use a proportionality constant to relate the difference between dynamic and statically measured P_c-S relationships to some measure of the rate of saturation or pressure change. Among these equations, the equation presented by *Hassanizadeh and Gray* [1993b] is one of the more widely used in the recent published literature. Based on thermodynamic theories and constitutive conservation laws, *Hassanizadeh and Gray* [1993b] derived equation (1):

$$P_c^d - P_c^s = -\tau \frac{\partial S}{\partial t}, \tag{1}$$

where P_c^s is the pressure difference between nonwetting and wetting phases within a porous medium under static (no flow) conditions (the true, or static capillary pressure), and P_c^d is the observed pressure difference between nonwetting and wetting phases within a porous medium under conditions where saturation is dynamically changing (the dynamic capillary pressure). It should be noted that some authors [e.g., *Bottero et al.*, 2011] have recently argued against the use of the term "dynamic capillary pressure" as it does not represent a true capillary pressure; we adopt this widely used terminology in the interest of concise discussion. It must be recognized, however, that P_c^d is not a true capillary pressure, but simply an observed pressure difference between phases under specific flow conditions. The parameter τ in equation (1), the dynamic capillary coefficient, is a measure of the magnitude of dynamic effects on measured capillary pressure. Larger values of τ correspond to a greater difference between P_c^d and P_c^s for a given rate of saturation change.

[7] Although a number of values of τ have been published, both from experimental and modeling studies, considerable uncertainty exists as to both its magnitude, and to how it is influenced by system properties. Published studies have reported values of τ for similar materials that differ by orders of magnitude. Based on eight published studies of dynamic effects dating from 1967 to 1998, *Hassanizadeh et al.* [2002] calculated approximate values of τ. Of the eight studies, seven involved drainage measurements in sands for air-water systems. However, despite the similarities in the porous media and fluids used, values ranged from 3×10^4 to 5×10^7 Pa s—a range of more than three orders of magnitude. More recent experimental studies in both air-water and organic liquid-water systems [e.g., *O'Carroll et al.*, 2005; *Oung et al.*, 2005; *Camps-Roach et al.*, 2010; *Sakaki et al.*, 2010; *Bottero et al.*, 2011; *Goel and O'Carroll*, 2011; *Das and Mirzaei*, 2012] have generally fallen within this range, but show little consistency between studies in terms of the effect of system properties (fluids, porous media) on magnitude of τ, how τ varies with saturation, or how it differs between drainage and imbibition. For example, *Sakaki et al.* [2010] report air-water drainage τ values for a fine sand that increase with decreasing saturation, reaching a value of approximately 10^7 Pa s at a saturation of 0.4. In contrast, *Camps-Roach et al.* [2010] report air-water drainage τ values for two similar sands which *decrease* with decreasing saturation, reaching a value of approx. 4×10^5 Pa s at $S \sim 0.6$—the opposite trend from that reported by *Sakaki et al.* [2010], and values one to two orders of magnitude lower. Furthermore, some authors have presented evidence suggesting that τ is higher for finer porous media [e.g., *Stauffer*, 1978; *Wildenschild et al.*, 2001; *Camps-Roach et al.*, 2010; *Das and Mirzaei*, 2012], while others have presented evidence that it is lower [e.g., *Oung et al.*, 2005].

[8] The overarching objective of this work was to explore dynamic capillary effects during drainage in unsaturated systems, with specific emphasis on understanding how τ varies with saturation and system properties during drainage. Two key differences between this work and earlier published studies are (1) this work makes use of extremely small (1.27 cm high) packed cells for measurements, and (2) all results include quantitative consideration of the effects of temporal sensor response and gas pressure gradients on calculated τ values.

[9] The use of a small packed cell eliminates larger-scale microheterogeneities that can occur in laboratory packing of porous media in larger columns, and also physically

limits the spatial range of sensors used for determining fluid pressures. *Bottero et al.* [2011] presented calculations showing that volume averaging of point measurements could produce measured τ values an order of magnitude higher than point measurements, a result that suggests that the spatial range of sensors used to make the measurements could potentially impact the resulting measured τ values. Most published experimental work examining dynamic effects has used packed columns ranging in height from approximately 10 cm [e.g., *Sakaki et al.*, 2010; *Bottero et al.*, 2011] to more than 50 cm [e.g., *Smiles et al.*, 1971; *Stauffer*, 1978]. In contrast, the cells used here have a height almost an order of magnitude smaller than most of the smallest columns used to date.

[10] Furthermore, it was hypothesized that the dynamics of both sensor response and gas pressure gradients could influence measured τ values by mimicking dynamic capillary effects under some conditions. As such, corrections for these potential artifacts are calculated for all experiments and their magnitudes explored.

2. Materials and Methods

2.1. Materials

[11] Two different unconsolidated porous media were used in this work: US Silica (Berkeley Spring, WV) F-95 Ottawa fine sand, and Scientific Industries (Bohemia, NY) SI-BG05 coarse glass beads. The properties of F-95 sand and glass beads are shown in Table 1. Properties of the F-95 sand are taken from *Chen et al.* [2007]. Due to the extremely high permeability of the coarse SI-BG05 glass beads, accurate measurement of permeability was not possible with our system (system conductivity is orders of magnitude lower than that of the glass beads themselves), so permeability of the glass beads was estimated using the Kozeny-Carman equation [*Bear*, 1972]. The two media were selected due to their extremely different d_{50} values, and correspondingly different capillary behavior. Prior to use, media were rinsed at least two times with deionized water to remove fines, and then oven dried.

[12] Two different wetting phases were used to explore the effects of wetting phase viscosity on dynamic capillary effects: Nanopure (Barnstead; Dubuque, IA) water, and a 35% w/v sucrose solution prepared with Nanopure water and standard table sugar. All experiments conducted for this work were conducted in unsaturated, gas-liquid systems, with gas as the nonwetting phase. The nonwetting phase in this study was high purity (≥99.99%) compressed nitrogen. Properties of all three fluids are given in Table 1. Viscosity and density of the sucrose solution were measured for this work, and are consistent with reported literature values.

Table 1. Properties of Porous Media and Fluids Used in Experiments[a]

Medium	d_{50} (mm)	Permeability κ (cm^2)
F-95 Sand	0.140	2.27×10^{-8}
SI-BG05 Glass Beads	0.629	1.88×10^{-6}
Fluid	**ρ (kg m^{-3})**	**μ (cP)**
Water	998	1.002
Sucrose Soln. (35% w/v)	1154	3.5
Nitrogen (g)	1.165	0.0178

[a]Fluid properties correspond to 20°C, atmospheric pressure.

2.2. System Description

[13] All experiments were conducted using an automated system modified from systems previously described by *Chen and Kibbey* [2006] and *Chen et al.* [2007]. The system makes use of a small volume, membrane-based soil cell for rapid control and measurement of capillary pressure and saturation in unconsolidated media. The system uses a computer-controlled servo-pressure regulator (type 3110, Marsh Bellofram, Newell, WV) to apply time-varying gas pressures to the top of the soil cell. Experiments start with a known liquid saturation in the cell (typically fully saturated), and as liquid drains from the cell it is collected in a vertical glass tube, where its volume is determined in real time from hydrostatic pressure. Saturation is calculated based on the known initial saturation and volume of liquid in a vertical glass tube. Full details of underlying system design and operation are provided by *Chen et al.* [2007].

[14] Figure 1 shows a diagram of the soil cell as modified for this work. The internal dimensions of the soil cell are 1.27 cm (height) × 2.54 cm (diameter) (a total internal volume of 6.44 mL, and a pore volume on the order of 2.3 mL, depending on porosity). A nylon membrane with a 20 μm pore size was used at the bottom of the cell as a water-wet capillary barrier, and a PTFE membrane with a 0.22 μm pore size was used at the top of the cell as a hydrophobic capillary barrier. Nylon membranes were purchased from GE Osmonics, Inc. (Minnetonka, MN), while PTFE membranes were purchased from Membrane Solutions (Plano, TX).

[15] For this work, two custom-designed fluid-selective pore pressure microsensors were integrated into the soil cells (Figure 1). The sensors are based on commercial

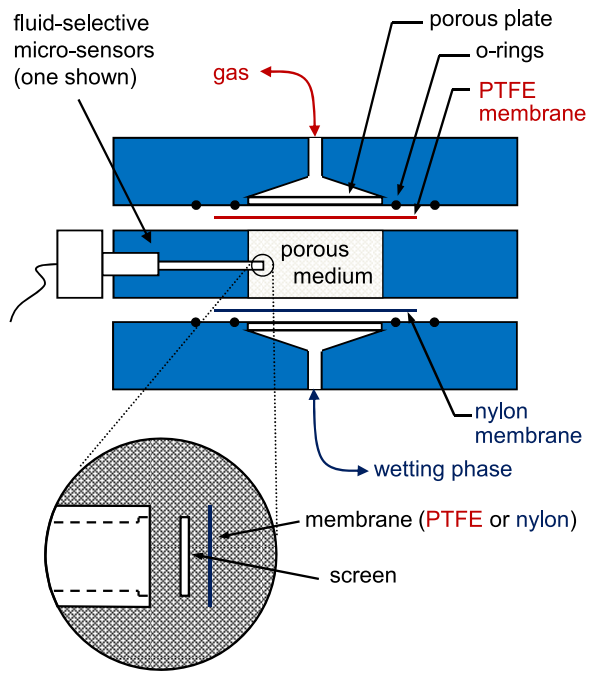

Figure 1. Exploded side view of soil cell with fluid-selective pore pressure microsensor. Second microsensor and microsensor drains not shown.

pressure transducers (PX481A or PX181, Omega Engineering, Inc., Stamford, CT), and are operationally similar to the sensors used by *Bottero et al.* [2011]. The commercial transducers connect to internal tubes which extend 3.5 mm into the interior of the cell. At the end of the tubes, 3.2 mm diameter countersunk #80 mesh stainless steel screens support fluid-selective membranes, which are glued in place with contact cement. For measurement of wetting phase pressures, nylon hydrophilic membranes with a pore size of 20.0 μm were used. For measurement of gas pressures, PTFE membranes with a pore size of 0.22 μm were used. For both types of measurement, the dead volume between the screen and the commercial pressure transducer was filled with degassed water and flushed through integrated drains to eliminate any gas behind the membranes. The reason for this is that for the microsensors to respond to a pressure change, a small amount of fluid must pass through the membrane for the fluid pressure to be registered by the commercial pressure transducer. Because of the high compressibility of gas, the presence of any gas behind the membrane can significantly slow the response of a fluid-selective pore pressure microsensor; this effect can be very significant with the fast sensors used for this work. For this reason, water was included behind the membrane even in sensors intended to measure gas pressures.

[16] Applied pressures were controlled by adjusting voltage to the servo-pressure regulator at 0.1 s intervals using a Measurement Computing (Middleboro, MA) PCI-DDA08/12 8-channel D/A board. Data from all sensors were acquired using a Measurement Computing PCI-DAS6034 A/D board. Data were read continuously at a rate of 12,288 samples s^{-1} per channel, and then continuously averaged over the most recent 1 s interval to smooth electronic noise. Data were recorded at 0.1 s intervals. For calculations involving data collected at different rates, all measurements were interpolated to saturation intervals of 0.001 (0.1%). All derivatives were calculated using central differences over a saturation window of ±0.02 (2%) about the desired saturation.

2.3. Experimental Procedures

[17] Cells were wet packed following procedures described by *Chen et al.* [2007]. A nylon membrane was initially placed on the top of the cell to allow degassed water to be flushed through the cell to dissolve any remaining trapped gas. Cells were flushed for approximately 15 pore volumes at a flow rate of 1 mL min^{-1}. Water flushed through the column was directed out of the bottom of the cell for the first approximately 5 pore volumes, and the remainder was directed out of the drains for the water-phase pore pressure microsensor(s).

[18] Following flushing, the top membrane was replaced with a PTFE membrane, and the response of the water-phase pore pressure microsensor was measured by closing the valve below the cell to prevent water flow, and then introducing a rapid pressure signal to the gas above the cell. Because there was no flow out of the cell, the change in applied gas pressure above the cell was transmitted directly to the water. Sensor response was found to be very well described by a first-order relationship (equation (2))

$$\frac{\partial P_s}{\partial t} = k(P - P_s), \tag{2}$$

where P_s is the pressure as detected by the sensor, P is the applied pressure of the phase of interest, and k is the first order rate constant describing sensor response. It should be noted that while the fluid-selective microsensors used in this work are used under positive pressures, their function is fundamentally the same as that of conventional tensiometers. Tensiometer response has been widely studied, and the first order response described by equation (2) has been observed for more than 60 years [e.g., *Richards*, 1949; *Klute and Gardner*, 1962; *Towner*, 1980]. The constant k in equation (2) is expected to be a function of both the porous medium and the sensor, although for media with sufficiently high permeabilities, sensor capillary barrier permeability dominates sensor response [e.g., *Klute and Gardner*, 1962; *Towner*, 1980; *Selker et al.*, 1992]. Measurements of gas phase sensor response were conducted separately on dry media. Note that separate preliminary tests with both types of sensors found no systematic variation in k over a wide range of saturations, with the exception of the gas sensors, which when initially wet (i.e., at the start of each drainage cycle) typically did not respond to external pressure changes until the pressure difference across the PTFE membrane reached approximately 60–70 cm water; this effect may be due to the rough surface of the PTFE membranes used, or water interaction with the polypropylene lamination, but was not found to impact rapid sensor response at the higher pressures. Note that the near-constant water sensor response with changing saturation observed here is consistent with a sensor whose response is not limited by the porous medium over the saturation range studied since decreasing conductivity with decreasing saturation would be expected to produce slower response at lower saturations in a porous medium-limited sensor [e.g., *Selker et al.*, 1992].

[19] Figure 2 illustrates the measurement of sensor response for three different water-phase sensors. The applied pressure in Figure 2 corresponds to a 210 cm water (2×10^4 Pa) change produced by a voltage step to the servo-pressure regulator. Because the system cannot produce an instantaneous pressure step of this magnitude, and because of the 1 s averaging smoothing used for noise reduction during all

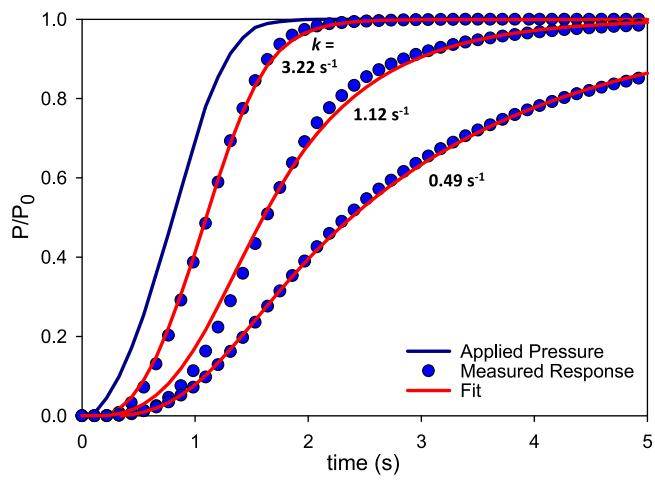

Figure 2. Water sensor response for three different membrane-based sensors. Numbers correspond to sensor first-order response rate constants (k; equation (2)).

data acquisition (section 2.2), the measured applied pressure (Figure 2) is used in place of a theoretical step input to calculate sensor response rate constants. (Note that the use of the same averaging smoothing for both the applied and sensor signals means that the resulting calculated sensor response constants are not impacted by the smoothing.) It should be noted that the sensors in Figure 2 respond extremely quickly compared with conventional tensiometers or ceramic-based fluid-selective sensors. For comparison, the sensors used by *Camps-Roach et al.* [2010] reached 95% of their final value in response to a step input after 120 s in unsaturated conditions, corresponding to a first order constant of $\sim$0.025 s^{-1}. Both *Bottero et al.* [2011] and *Sakaki et al.* [2010] report that their fluid-selective pressure sensors responded to pressure changes faster than those in Figure 2, but they do not provide detailed rate information. From a practical standpoint, it can be difficult to accurately determine rate constants for sensors with k faster than $\sim$4 s^{-1}, simply because it is difficult to create a rapid enough input pressure change. Note that the differences in the three sensors in Figure 2 likely result from slight differences in the amount of glue used to attach the membranes, and may also result from small air bubbles trapped in the dead volume between the membrane and the transducer. Other factors that can influence sensor response include fluid viscosity (higher viscosity fluids produce slower response) and membrane permeability (low permeability membranes produce slower response).

[20] Following characterization of water-phase microsensor response, dynamic experiments were conducted as follows. All experiments made use of ramped pressure inputs, both for imbibition and drainage. For all porous media, a slow pressure ramp (approximately 0.05 cm water s^{-1}) was used to produce primary drainage and main imbibition. After main imbibition, a total of seven secondary drainage/imbibition cycles were performed, with drainage rates increasing from $\sim$0.1 to $\sim$7.5 cm water s^{-1} (exact values varied slightly depending on which servo-pressure regulator was used). Imbibition after each secondary drainage was conducted at a slow 0.1 cm water s^{-1} rate. After each drainage and imbibition, pressure was held constant for 20 s to allow for any additional equilibration of fluids between cycles. Calculations exploring dynamic capillary effects were conducted using pressure measurements made during the secondary drainages. The inherent assumption of this approach is that the water configuration at the start of each drainage is essentially the same, regardless of previous cycles. This assumption is supported by the fact that the starting saturation for each secondary drainage was nearly the same for all experiments (within approximately 2%). Furthermore, preliminary experiments conducted with decreasing (fast to slow) instead of increasing (slow to fast) pressure rates produced results that were virtually identical to those presented here, providing confidence in the approach and the results.

[21] A total of three different experiments were conducted for the work: two in F-95 sand (one with water, one with sucrose solution), and one in coarse glass beads with water (Table 2). All experiments made use of two fluid-selective pore pressure microsensors. One experiment (Expt. 1, F-95/water) included one water-phase microsensor and one gas-phase microsensor, while the other two experiments each included two water-phase microsensors, each with a different response rate. All experiments were conducted at room temperature (approximately 22 $\pm$ 1°C).

2.4. Calculations

[22] To better understand the impact of potential measurement artifacts on the calculation of τ, we explore the magnitudes of quantitative corrections for sensor response, as well as pressure drop in the column due to gas flow. Corrections are used to calculate estimates of true (corrected) pressures inside the cell based on either measured sensor or influent pressures.

[23] Correction from sensor response is made using equation (3) (a rearrangement of equation (2)):

$$P^i_{\text{corr.(sens.)}} = \frac{1}{k^i}\frac{\partial P^i_s}{dt} + P^i_s, \tag{3}$$

where $P^i_{\text{corr.(sens.)}}$ is the estimated true pressure in the cell for phase i (water or gas). Because all of the items on the right-hand side are known, it is possible to calculate $P^i_{\text{corr.(sens.)}}$ at every experimental time step. Note that this correction is identical to the approach described by *Klute and Gardner* [1962] for dynamic correction for tensiometer response. The impact of this correction is greatest for systems with slower sensors, and where rates of pressure change are greatest.

[24] Correction for gas flow is made to better understand the impact of using influent gas pressures on calculation of τ. Others have made measurements based on the assumption that gas can be considered infinitely mobile in the column. However, it was hypothesized that for some systems this assumption may not be satisfied. To correct for pressure drops in the gas, we ignore compressibility and assume that volumetric gas flow into the cell is equal to volumetric water flow out of the cell, and then use Darcy's law to estimate the pressure drop between the top of the cell and the vertical midpoint of the cell (the location of the fluid-selective pore pressure microsensors) (equation (4)):

$$P^g_{\text{corr.(flow.)}} = P^g_{\text{inlet}} - \frac{q_w L}{\kappa k_{\text{rnw}}(S)}\frac{\mu_g}{\rho_w g}, \tag{4}$$

where $P^g_{\text{corr.(flow.)}}$ and P^g_{inlet} are the estimated true pressure in the cell and the measured inlet gas pressure at a given

Table 2. Experiment Conditions and Sensor Response Rate Constants

Experiment	Medium	Wetting Fluid	Porosity (n)	P_g max (cm water)	Cycles (2° dr.)	Sensor Rate Constants (s^{-1})		
						k^g	k^w-A	k^w-B
1	F-95 Sand	Water	0.36	190	7	3.0	3.2	–
2	F-95 Sand	Sucrose Solution	0.36	198	7	–	0.59	0.40
3	SI-BG05 Glass Beads	Water	0.37	140	7	–	1.12	0.49

experimental time step, both in units of height of water ($\rho_w g$ converts the pressures to water height units). The Darcy velocity of water leaving the cell is given by q_w, the distance from the inlet of the cell to the vertical midpoint is L (6.35 mm in this case), the permeability of the medium and gas viscosity are κ and μ_g, respectively (Table 1). Relative permeability of the nonwetting phase (k_{rnw}) was calculated using the relationship described by *Brooks and Corey* [1966] (a relationship that has been found to provide very good estimates of k_{rnw} [e.g., *Fischer et al.*, 1997]:

$$k_{\mathrm{rnw}} = (1 - Se)^2 \left(1 - Se^{[1+(2/\lambda)]}\right), \tag{5}$$

where Se is effective saturation [$Se = (S - Swr)/(snwr - Swr)$, where S_{nwr} is water saturation corresponding to nonwetting phase residual], and λ is the pore size distribution index from the Brooks-Corey fit to the capillary pressure-saturation relationship. Equation (4) can be considered approximate, and is most appropriate for a very small cell, where saturation can be expected to be near uniform at all but the highest saturations, particularly during secondary drainage; corrections in longer columns would require a more complex approach taking into account vertical gradients in saturation (and, as a result, gradients in gas permeability). The impact of the correction described by equation (4) is greatest for systems with low permeabilities, but over saturation ranges where flow rates are high.

2.4.1. Dynamic Capillary Pressures

[25] Calculation of τ (equation (1)) requires values of dynamic capillary pressure at each saturation where the calculation is conducted. For this work we define four different dynamic capillary pressures based on the corrections described in equations (3) and (4). Table 3 provides the definitions of the four dynamic capillary pressures. In cases where a second water phase sensor is used in place of a gas phase sensor (Expts. 2 and 3 (Table 2)), P_c^d-1 and P_c^d-1* are calculated for each of the two sensors, and are identified with A or B, to match the sensor designations in Table 2.

2.4.2. Calculation of τ

[26] To calculate the dynamic capillary coefficient τ we rearrange equation (1) into equation (6):

$$P_c^d(S)|_j = -\tau(S)\frac{\partial S}{\partial t}(S)\bigg|_j + P_c^s(S), \tag{6}$$

where the index j corresponds to data from a drainage curve conducted at a specific rate. Based on equation (6), it is apparent that plots of $P_c^d(S)$ versus $\frac{\partial S}{\partial t}(S)$ at a given saturation should give a linear relationship, with a slope equal to $-\tau(S)$ and an intercept equal to the static capillary pressure $P_c^s(S)$. Because the experiments conducted for this work do not involve direct measurement of P_c^s, equation (6) is used to measure τ based on the data from seven dynamic drainage curves. A program specifically written for the purpose conducts regressions across all saturations (at 0.001, or 0.1% saturation increments). The program also calculates standard error of the regression at each saturation. Calculated values of τ are reported as τ_1, τ_1^*, τ_2, τ_2^*, depending which P_c^d value (Table 3) is used in the calculation.

3. Results and Discussion

3.1. F-95 Sand/Water

[27] Figure 3 shows both the time evolution of saturation (dotted lines) and calculated $\frac{\partial S}{\partial t}$ as a function of saturation for the F-95 sand/water system (Expt. 1). Results shown correspond to seven secondary drainage curves conducted at ramped gas pressure rates spanning almost two orders of magnitude (~0.1 to ~7.6 cm water s^{-1}). Each curve corresponds to drainage that occurs during each ramp up to the specified maximum gas pressure (190 cm water in this case (Table 2)). These experimental conditions produce drainage curves that take between ~20 and 1000 s to complete, and maximum rates of saturation change $\left(\frac{\partial S}{\partial t}\right)$ that vary from approximately -0.0013 s^{-1} for the slowest drainage to -0.03 s^{-1} for the fastest curve.

[28] Figure 4 shows the uncorrected pressures for the F-95 sand/water system (Expt. 1) measured in the influent gas (solid lines) and by the water phase pore pressure microsensor (dotted lines) for the same seven drainage curves. Note that the use of a ramped pressure input with this system produces a case where both water and gas pressures increase during drainage. The flow-through system used by *Bottero et al.* [2011] produces a similar result during the measurement process, with the pressures in both phases increasing with decreasing saturation. In contrast, the system used by *Camps-Roach et al.* [2010] (and others like it which use a constant gas pressure or water vacuum input) produces constant gas pressure and decreasing water pressures with decreasing saturations. In cases where temporal sensor response impacts measured dynamic capillary effects, it is likely that the direction of pressure change is significant, as a lagging sensor will over- or under-predict pressures, depending on the direction of the lag.

[29] Figure 5 shows measured dynamic capillary pressures for the F-95 sand/water system (Expt. 1), calculated

Table 3. Definitions of the Four Different Dynamic Capillary Pressures ($P_c^d = P_g^d - P_w^d$) Used in Calculations

	Gas Pressure (P_g^d)				Water Pressure (P_w^d)	
	Influent Gas Pressure		Gas Microsensor		Water Microsensor	
P_c^d	Uncorrected	Corrected (Equation (4))	Uncorrected	Corrected (Equation (3))	Uncorrected	Corrected (Equation (3))
P_c^d-1	X				X	
P_c^d-1*		X				X
P_c^d-2			X		X	
P_c^d-2*				X		X

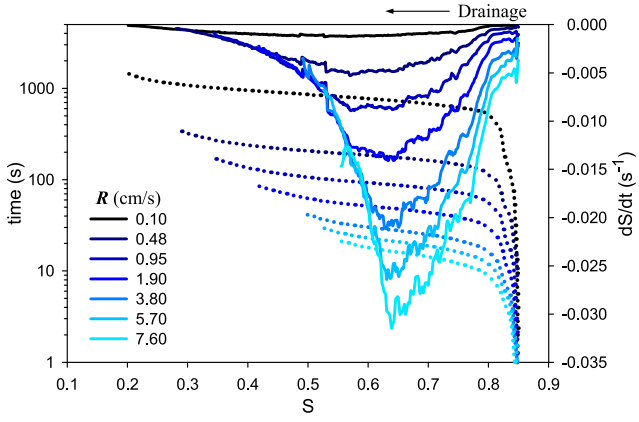

Figure 3. $\partial S/\partial t$ (solid lines) and elapsed time (dotted lines) for drainage at different applied ramped gas pressure rates (R). Curves correspond to secondary drainages of F-95 sand initially saturated with water (Expt. 1).

based on the definitions in Table 3. For comparison, apparent capillary pressures (the pressure difference between phases across the cell inlet and outlet) are also shown as an inset (Figure 5e, dotted lines). Note that apparent capillary pressures are much greater than the other pressures because they include the pressure gradient in the water phase that results from flow.

[30] Figures 5a and 5b correspond to dynamic capillary pressures calculated based on uncorrected pressures. The dynamic capillary pressure based on influent pressure (P_c^d-1; Figure 5a) looks like many (but not all) of the published dynamic capillary pressure curves from the past four decades, in that the curves deviate from one another to the greatest extent at higher saturations, but converge on a single curve at lower saturations [e.g., *Topp et al.*, 1967; *Smiles et al.*, 1971; *Vachaud et al.*, 1972; *Stauffer*, 1978; *Kalaydjian*, 1992; *Bottero et al.*, 2011]. In contrast, the dynamic capillary pressure based on the two uncorrected internal sensors (P_c^d-2; Figure 5b) shows very little difference between any of the curves, except at the highest saturations, where no gas sensor response is observed at the start of drainage. (As mentioned previously, measurements show that the gas sensors used for Expt. 1 do not respond until gas pressure difference across the PTFE membrane exceeds approximately 60–70 cm water.)

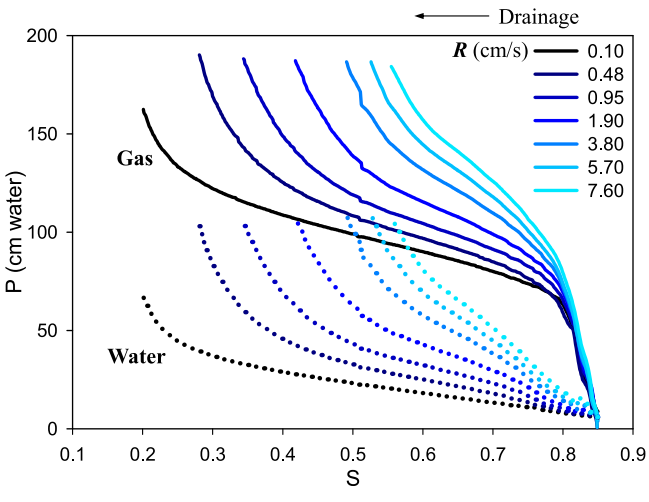

Figure 4. Inlet gas pressures (solid lines) and measured water pressures (dotted lines) for drainage at different applied ramped gas pressure rates (R). Curves correspond to secondary drainages of F-95 sand initially saturated with water (Expt. 1).

[31] Figures 5c and 5d show corrected dynamic capillary pressures calculated using the corrections described in equations (3) and (4). Examination of both figures shows that the corrected values come very close to collapsing onto the same curve. This is particularly notable for P_c^d-1* (Figure 5c), given how far apart the P_c^d-1 curves were in Figure 5a. Note that the magnitude of the correction in Figure 5c can be attributed approximately 40% to water sensor response, and 60% to gas flow, when considered at $S = 0.7$. However, the relative magnitudes of the two corrections differ at different saturations, with the flow correction decreasing monotonically with decreasing saturation (as a result of increasing gas permeability), and the sensor correction remaining relatively constant over much of the saturation range after an initial increase at high saturations.

[32] In the case of P_c^d-2* (Figure 5d), while the curves do come very close to collapsing on one another, there is little difference from the uncorrected P_c^d-2 (Figure 5b). It is important to note that this situation is entirely due to the fact that the two sensors in this case happen to be very closely matched ($k^w = 3.2$ s^{-1}, $k^g = 3.0$ s^{-1}). That means that sensor lag in each of the two phase pressures essentially cancels the other out, causing uncorrected P_c^d-2 curves to closely approximate corrected P_c^d-2* curves. It is important to emphasize, however, that any mismatch in sensor response could potentially cause significant differences. For example, even though both sensors are extremely fast ($k = 3.0$ s^{-1} corresponds to a 50% response to a stepped input in approximately 0.2 s), if one of the two were infinitely fast, the fastest uncorrected curve in Figure 5d would shift up or down by approximately 3 cm water, depending on which sensor had the instantaneous response. Similarly, if one of the two sensors were much slower than the other (e.g., due to viscosity differences), the differences in measured P_c^d-2 curves could be much more significant.

[33] As mentioned previously, calculation of τ is done by regression of equation (6) at 0.001 saturation intervals. Figure 6 illustrates the regression at three specific saturations for the F-95 sand/water system (Expt. 1), for calculation of τ_1 from P_c^d-1 (separate regressions are conducted for each of the four different dynamic capillary pressures (Table 3)).

[34] The results of regressions for Expt. 1 are shown in Figure 7. Note that error bars in Figure 7 correspond to the standard error of the regression slope ($-\tau$) at each saturation. As such, it is important to emphasize that error bars are primarily a measure of the uncertainty of τ resulting from the regression itself (i.e., deviation from linearity), rather than a comprehensive indication of uncertainty in τ.

[35] From Figure 7 it is apparent that τ_1, the dynamic capillary coefficient calculated from uncorrected influent pressure and uncorrected water sensor pressure (i.e., P_c^d-1), has the greatest magnitude, approaching 10^5 Pa s at high saturations. It is also apparent that τ_1 exhibits a decreasing

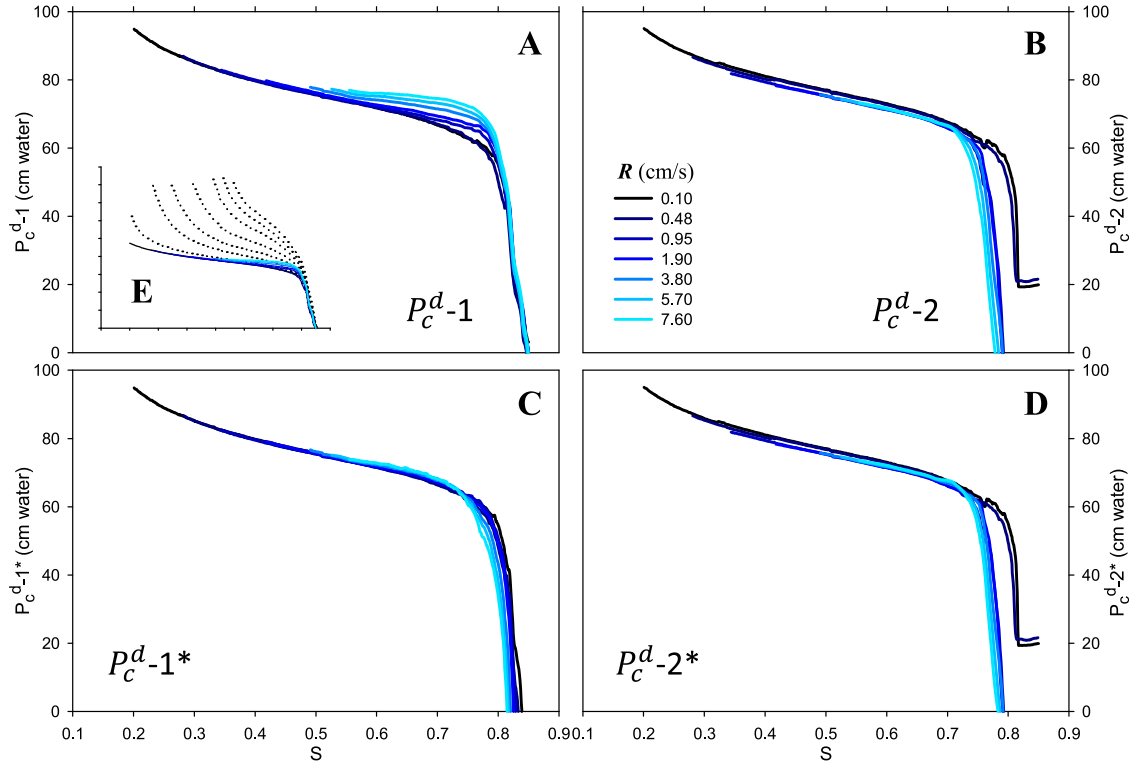

Figure 5. (a and b) Uncorrected, (c and d) corrected, and (e) apparent dynamic capillary pressures, calculated based on the definitions in Table 3. Curves correspond to secondary drainages of F-95 sand initially saturated with water (Expt. 1).

trend with decreasing saturation; this trend is almost entirely attributable in this system to the use of influent gas pressure, because the difference between influent gas pressure and pressure at the midpoint of the porous medium decreases with decreasing saturation. However when pressures are corrected for gas flow and water sensor response (i.e., P_c^d-1*), the corresponding dynamic capillary coefficient $\left(\frac{\partial S}{\partial t}\right)$ is considerably lower, exhibiting a relatively constant magnitude of $\sim 5 \times 10^3$ Pa s over much of the saturation range. Note that τ_1^* is actually calculated to be negative at the highest saturations; this is the result of the simplified gas flow correction (equation (4)) over-predicting the

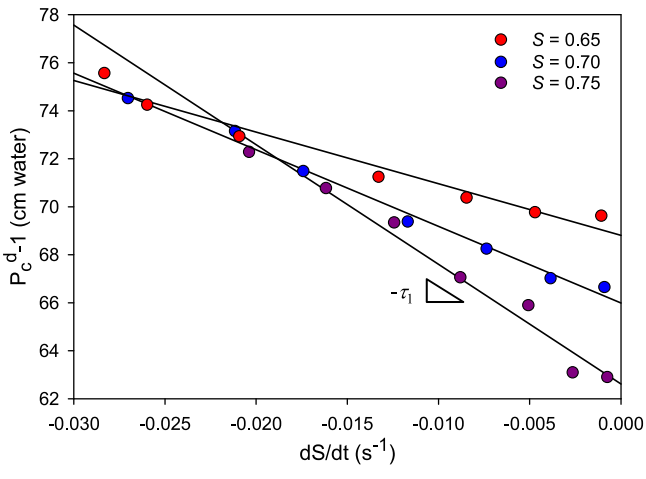

Figure 6. Illustration of regression used to determine τ values, shown for three saturations for F-95 sand initially saturated with water (Expt. 1). Actual analyses involve regressions at saturation intervals of 0.001.

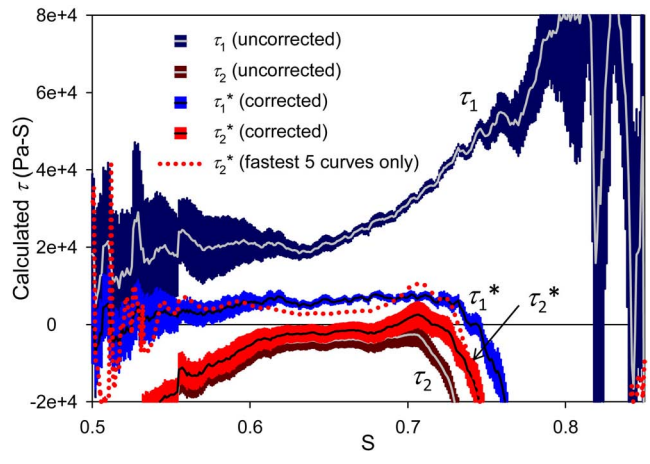

Figure 7. Calculated uncorrected and corrected τ values for F-95 sand initially saturated with water (Expt. 1). Values correspond to the definitions of P_c^d in Table 3. Error bars correspond to standard error of the regression at each saturation.

correction for gas flow pressure drop at high saturations, causing inversion of P_c^d-1* curves at high saturations (Figure 5c).

[36] Calculated values for τ_2 and τ_2^* shown in Figure 7 are very similar to one another. This might be expected because of the similarities between the corresponding dynamic capillary pressures used in their calculation (P_c^d-2 and P_c^d-2*; Figures 5b and 5d). Because the gas sensor does not respond at high saturations (Figure 5c), both calculated τ values exhibit significant negative magnitudes at the highest saturations. Note, however, that both values actually remain negative (although close to zero) over much of the saturation range. Close examination of the P_c^d-2 plots in Figure 5b shows that the gas pressure microsensor may actually have experienced a small offset after the first two (the slowest two) secondary drainage curves, in that all curves after the first (fastest) two are approximately 2 cm water lower than the first two. This is an occasional issue with both types of sensors. (Also note the lower starting pressures in the five faster runs (Figures 5b and 5d)) When τ_2^* is recalculated using only the five faster drainages (Figure 7, dotted red line), its shape and magnitude are *very* close to those of τ_1^*.

[37] The results in Figure 7 suggest that the true magnitude of τ for the F-95 sand/water system studied here is likely on the order of $\sim 5 \times 10^3$ Pa s at the most, and may actually be lower. Furthermore, the results in Figure 7 highlight the potential for measurement artifacts to introduce order-of-magnitude errors in the calculation of τ, even when extremely fast sensors are used.

3.2. F-95 Sand/Sucrose Solution

[38] Figure 8 shows measured dynamic capillary pressures for the F-95 sand/sucrose solution system (Expt. 2), calculated based on the definitions in Table 3. For comparison, apparent capillary pressures (the pressure difference between phases across the cell inlet and outlet) are also shown as an inset (Figure 8e). For this experiment, a second wetting-phase sensor was used in place of a gas sensor. As such, the curves in Figures 8a and 8c correspond to P_c^d-1A and P_c^d-1A*, respectively, and the curves in Figures 8b and 8d correspond to P_c^d-1B and P_c^d-1B*, respectively. From the sensor response rate constants in Table 2, it can be seen that the sensor responses are considerably different from one another (A is faster than B), and are both considerably slower than the water sensor used in Expt. 1 (k^w of 0.59, 0.40 versus 3.2 s^{-1} in Expt. 1). The slower rate compared with Expt. 1 can likely be attributed in part to the 3.5× higher viscosity of the sucrose solution (Table 1). Unlike Expt. 1 (Figure 5), it can be seen that neither P_c^d-1A (Figure 8a) or P_c^d-1B (Figure 8b) completely converge at lower saturations, but rather are shifted higher at higher rates. The differences between P_c^d-1A and P_c^d-1B are consistent with the differences in wetting-phase sensor response rate constants, with the slower sensor (Figure 8b) creating the appearance of significantly higher dynamic capillary pressures for the same drainage process—a nearly 10 cm water difference at the fastest rate. It is important to emphasize that although these sensors are slower than the sensor used in Expt. 1, and differ considerably from one another, both are still very fast sensors. In fact, sensor A

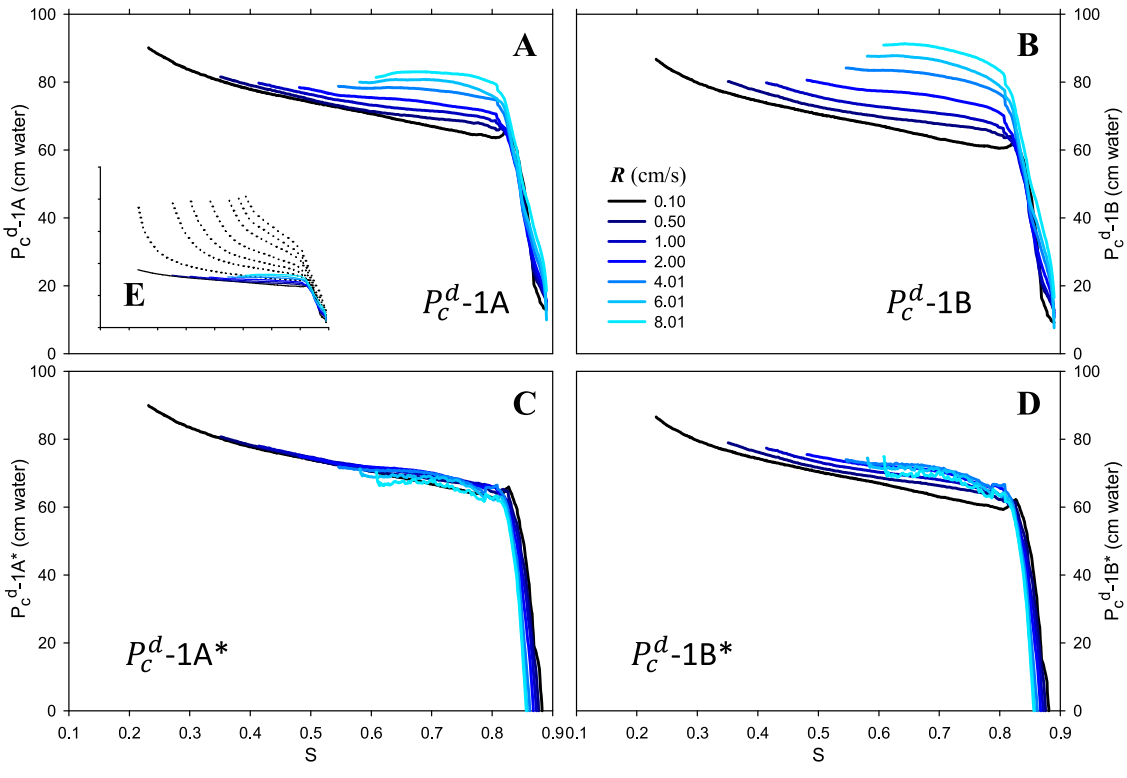

Figure 8. (a and b) Uncorrected, (c and d) corrected, and (e) apparent dynamic capillary pressures, calculated based on the definitions in Table 3. Curves correspond to secondary drainages of F-95 sand initially saturated with sucrose solution (Expt. 2).

would exhibit a 50% response to a step input in only 1.2 s, while sensor B would exhibit a 50% response to a step input in only 1.7 s.

[39] Figures 8c and 8d show the impact of correction for gas flow pressure drop and wetting phase sensor response for the two sensors. In the case of the faster sensor, where the required correction is smaller, the corrected curves collapse onto one another (Figure 8c). For the slower sensor, where the correction is larger, the curves do not completely collapse onto one another (Figure 8d), but are considerably closer than the uncorrected curves (Figure 8b). Note that the magnitude of the gas flow correction is slightly smaller to that for the F-95/water system (due to slower flow rates), but the slower sensor response in the F-95/sucrose means the sensor correction is much more significant. For the faster of the two sensors (A), the sensor pressure correction makes up approximately 90% of the total correction at $S = 0.7$. This is in contrast to the 40% water sensor correction contribution in the F-95/water system.

[40] Figure 9 shows calculated τ values corresponding to the four dynamic capillary pressures from Figure 8. As might be expected, the τ values based on uncorrected dynamic capillary pressures (τ_{1A} and τ_{1B}) are significantly greater than the τ values based on corrected dynamic capillary pressures ($\tau_{1A}{}^*$ and $\tau_{1B}{}^*$). Furthermore, the uncorrected value corresponding to the slower of the two sensors (τ_{1B}) is almost twice the magnitude of the uncorrected value corresponding to the faster of the two sensors (τ_{1A}), and both values are considerably higher than the uncorrected values for the F-95/water system (Figure 7). It is also interesting to note that neither uncorrected curve exhibits the decreasing τ with decreasing saturation that was observed in Figure 7. The primary reason for this is the much greater contribution of slow sensor response (rather than gas flow) to creating the appearance of dynamic capillary effects in the uncorrected F-95/sucrose solution system (Figure 9) compared with the F-95/water system (Figure 7).

[41] As might be expected from the corrected dynamic capillary pressures in Figures 8c and 8d, the dynamic capillary coefficients calculated from the corrected pressures ($\tau_{1A}{}^*$ and $\tau_{1B}{}^*$) are relatively small in magnitude. This is particularly true for $\tau_{1A}{}^*$, which corresponds to the faster of the two sensors, and for which the corresponding corrected dynamic capillary pressures (Figure 8c) come very close to collapsing to a single curve. The magnitude of $\tau_{1A}{}^*$ is between approximately 0 and $\sim 2 \times 10^3$ Pa s over much of the saturation range shown, although the standard error of the regressions overlaps 0 for nearly the entire range. The magnitude of $\tau_{1B}{}^*$ is higher, on the order of $\sim 2 \times 10^4$ Pa s over much of the saturation range shown, but still small compared with the uncorrected value. It should also be noted that the 95% confidence intervals (not shown in Figure 9 for clarity, but 2.57× the standard errors shown) for both corrected values ($\tau_{1A}{}^*$ and $\tau_{1B}{}^*$) overlap one another, suggesting the values are not statistically different from one another.

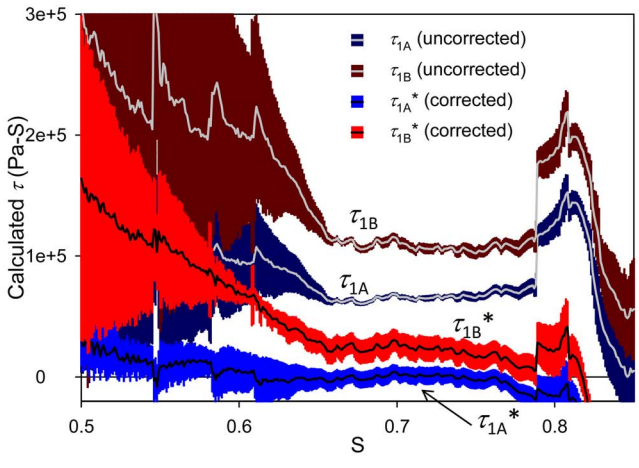

Figure 9. Calculated uncorrected and corrected τ values for F-95 sand initially saturated with sucrose solution (Expt. 2). Values correspond to the definitions of P_c^d in Table 3. Error bars correspond to standard error of the regression at each saturation.

3.3. Si-BG05 Glass Beads/Water

[42] Figure 10 shows measured dynamic capillary pressures for the SI-BG05 glass beads/water system (Expt. 3), calculated based on the definitions in Table 3. For comparison, apparent capillary pressures (the pressure difference between phases across the cell inlet and outlet) are also shown as an inset (Figure 10e). As was the case for Expt. 2, a second wetting-phase sensor was used in place of a gas sensor for this experiment. As such, the curves in Figures 10a and 10c correspond to P_c^d-1A and P_c^d-1A*, respectively, and the curves in Figures 10b and 10d correspond to P_c^d-1B and P_c^d-1B*, respectively. As was the case in Expt. 2, the two water sensor responses are considerably different from one another (A is faster than B). The faster of the two sensors is slightly slower than the F-95/water system (Expt. 1), but faster than the faster sensor in the F-95/sucrose solution system (Expt. 2).

[43] Like Expt. 2 (Figure 8), it can be seen that neither P_c^d-1A (Figure 10a) or P_c^d-1B (Figure 10b) converge at lower saturations, but rather are shifted higher at higher rates. The differences between P_c^d-1A and P_c^d-1B are consistent with the differences in wetting-phase sensor response rate constants, with the slower sensor (Figure 10b) creating the appearance of significantly higher dynamic capillary pressures for the same drainage process—a nearly 15 cm water difference at the fastest rate. This error is approximately 50% greater than was observed for the slow sensor in the F-95/sucrose experiment (Expt. 2), primarily because the faster drainage rate in the glass beads/water system leads to more rapid water pressure changes, and consequently greater sensor lag, despite the faster sensor.

[44] Figures 10c and 10d show the impact of correction for gas flow pressure drop and wetting phase sensor response for the two sensors. In both cases, the corrected curves collapse onto one another. Note that the noise in the fast curves, most notable in the fastest curve of Figure 10d, is simply amplification of signal noise in the sensor pressure derivative (equation (3)), apparent here because the correction is so significant (~15 cm water correction on a ~10 cm water P_c—approximately 150% of the final value). Unlike the two experiments conducted in sand, the water sensor correction (equation (3)) makes up nearly all of the correction (>99.7% at $S = 0.7$). This is because the permeability

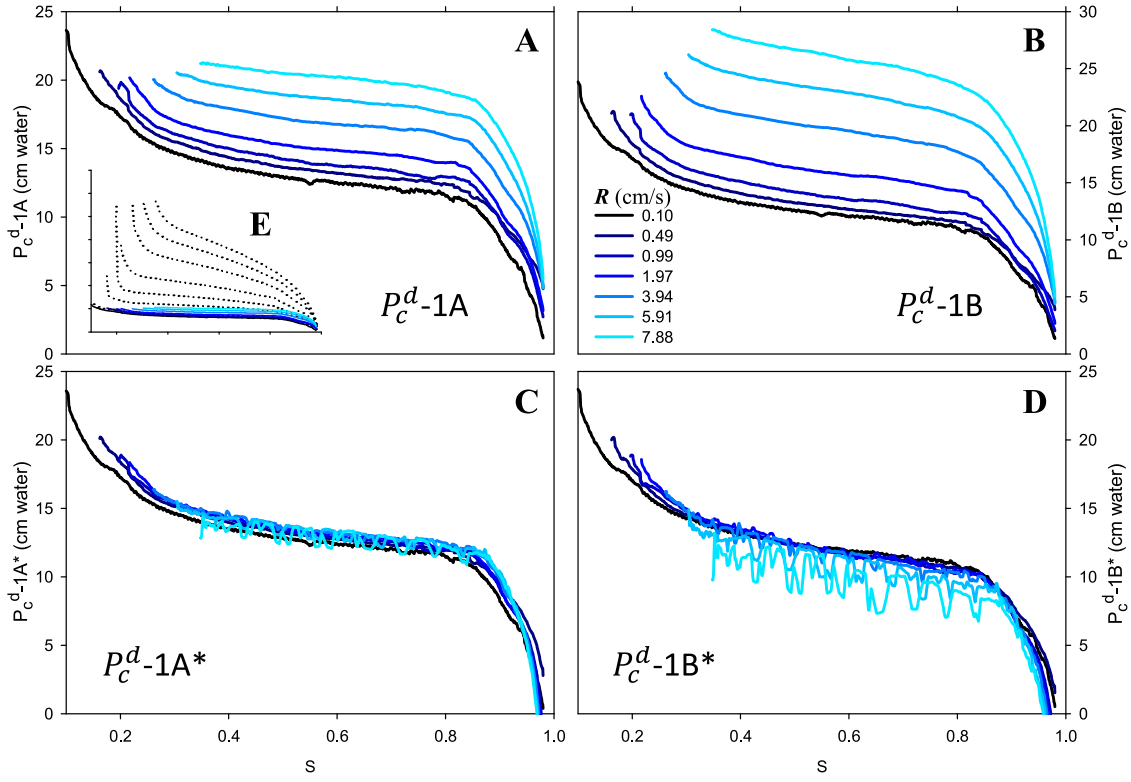

Figure 10. (a and b) Uncorrected, (c and d) corrected, and (e) apparent dynamic capillary pressures, calculated based on the definitions in Table 3. Curves correspond to secondary drainages of SI-BG05 glass beads initially saturated with water (Expt. 3).

of the glass beads is much greater, so the resistance to gas flow at the measured Darcy velocities is negligible.

[45] Figure 11 shows calculated τ values corresponding to the four dynamic capillary pressures from Figure 10. As might be expected, the τ values based on uncorrected dynamic capillary pressures (τ_{1A} and τ_{1B}) are significantly greater than the τ values based on corrected dynamic capillary pressures

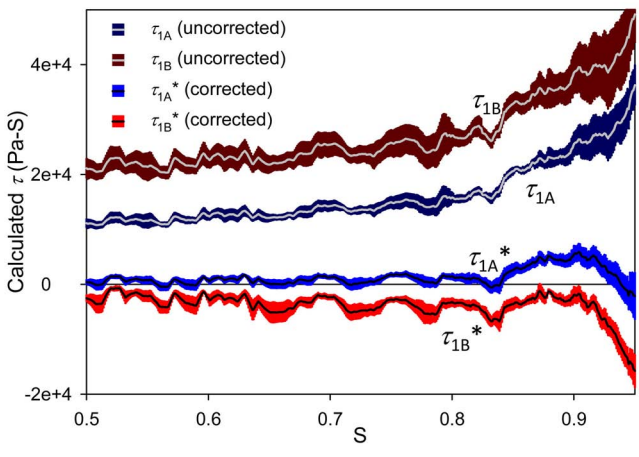

Figure 11. Calculated uncorrected and corrected τ values for SI-BG05 glass beads initially saturated with water (Expt. 3). Values correspond to the definitions of P_c^d in Table 3. Error bars correspond to standard error of the regression at each saturation.

($\tau_{1A}{}^*$ and $\tau_{1B}{}^*$). Furthermore, the uncorrected value corresponding to the slower of the two sensors (τ_{1B}) is considerably greater than the magnitude of the uncorrected value corresponding to the faster of the two sensors (τ_{1A}). Both uncorrected values are lower than the comparable τ value for the F-95/water system (τ_1; Figure 7). It is also apparent that, if viewed on the same scale, the uncorrected τ curves for the glass beads are considerably flatter than those for the sand—the result of the negligible gas flow correction. (Note that a slow sensor does impose a small decrease in τ with decreasing saturation at high saturations, but the effect is small compared with the gas flow correction.)

[46] As might be expected from the corrected dynamic capillary pressures in Figures 10c and 10d, the dynamic capillary coefficients calculated from the corrected pressures ($\tau_{1A}{}^*$ and $\tau_{1B}{}^*$) are very small in magnitude. The magnitude of $\tau_{1A}{}^*$ is between approximately 0 and $\sim 1 \times 10^3$ Pa s over much of the saturation range shown, while the magnitude of $\tau_{1B}{}^*$ is actually slightly negative.

3.4. Measurement Artifacts in Unsaturated Systems

[47] The results of these experiments suggest that measurement artifacts may make a significant impact on the determination of the dynamic capillary coefficient τ from experimental data. Even extremely fast sensors have the potential to create the appearance of dynamic capillary effects if their rates are mismatched (or if a sensor is used in only one phase, creating the same effect as mismatched sensors). In cases where only a water phase sensor is used, an additional artifact which can impact calculations is

pressure drops in the flowing gas. Our measurements with a stagnant water phase show very rapid response of gas sensors (e.g., Table 2, Expt. 1). However, when water is draining, the accompanying flow of gas produces pressure drops that can be significant, depending on the permeability of the medium. For the work here, which used a very small soil cell, a simplified correction was used (equation (4)) to correct for the pressure drop in the gas. The fact that calculations of τ made using that correction (τ_1^*; Figure 7) are in close agreement with the two-sensor measurements (τ_2^*; Figure 7), supports both the magnitude and underlying physics of the correction. In a larger column, where measurements are made on a moving front, pressure drops are likely to be most significant near the front. Preliminary unsaturated flow simulations conducted for this work show that, even for a porous medium with an order of magnitude higher permeability than F-95 sand (e.g., the sand used by *Sakaki et al.* [2010]), gas pressure drops of one to several cm water near the front are highly likely for typical Darcy velocities reported—an error that could create the appearance of a very large τ.

[48] It is interesting to note that the artifacts described here are themselves both scale dependent and system dependent, facts that may contribute to the significant variability in published τ values. In terms of system dependencies, the relationship between system backpressure and medium permeability can change the relative importance of sensor and flow artifacts. A system with a higher backpressure will artificially reduce the gas pressure drop in the medium compared with what would be observed for the same medium in a low-backpressure system, because the system itself (e.g., tubing, membranes) will dominate the water flow, creating a flatter τ-S relationship.

[49] In terms of scale dependence, it is very interesting to note that the relationship between water Darcy velocity at the outlet (q) (or, approximately equivalently, gas-phase Darcy velocity at the inlet) and the rate of saturation change $\frac{\partial S}{\partial t}$ can depend significantly on column length for an unsaturated system. By mass balance, q is related to the average saturation change over the entire column by equation (7):

$$q = nL\frac{\partial S}{\partial t}\Big|_{\text{avg}}, \tag{7}$$

where n is porosity, and L is the length of the column. Although the local rate of saturation change can potentially be much larger than the average, in practice in air/water systems unless a column is very long (i.e., $L \gg$ air entry pressure) or the P_c-S relationship is extremely sharp, the maximum local rate of saturation change $\frac{\partial S}{\partial t}$ is likely to be reasonably well approximated by the maximum average rate of saturation change $\frac{\partial S}{\partial t}\big|_{\text{avg}}$. (This result has been verified with unsaturated flow modeling, and is because of the significant fluid viscosity differences in air/water systems; this result will *not* generally be true for liquid/liquid systems). For example, analysis of the outflow and S versus time data published by *Camps-Roach et al.* [2010] for unsaturated drainage of a 20 cm long column packed with a coarse sand shows that the maximum local $\frac{\partial S}{\partial t}$ is only approx. 6% greater than the maximum $\frac{\partial S}{\partial t}\big|_{\text{avg}}$ calculated from outflow data. (In contrast, the liquid/liquid data of *Bottero et al.* [2011] show an order of magnitude difference between the local and average rates.) Taken together with equation (7), this result means that for a given q, a longer unsaturated column is likely to have a much lower maximum local $\frac{\partial S}{\partial t}$. Consider a comparison between the q and $\frac{\partial S}{\partial t}$ of *Camps-Roach et al.* [2010] and the F-95/water data (Expt. 1) presented here. The $R = 0.95$ cm s^{-1} $\frac{\partial S}{\partial t}$ curve in Figure 3 (Expt. 1, F-95/water) exhibits a maximum $\frac{\partial S}{\partial t}$ of approximately 0.008 s^{-1}, corresponding to a q of $\sim 3.5 \times 10^{-5}$ m s^{-1}. In contrast, the *Camps-Roach et al.* [2010] data (F32/50 sand, 132 cm water gas pressure) exhibit a very similar q ($\sim 3.9 \times 10^{-5}$ m s^{-1}), but a maximum $\frac{\partial S}{\partial t}$ of approximately 0.00065 s^{-1}—lower than our system by a factor that is very close to the ratio of column lengths (20/1.27 cm = 15.7). The reasons this is important are that sensor artifacts are controlled by rates of pressure change, which closely track rates of saturation change, while gas flow artifacts are controlled by Darcy velocity. As such, changing the length of a column for the same material changes the potential contribution of different potential artifacts. Furthermore, the lower $\frac{\partial S}{\partial t}$ in a longer column for a given Darcy velocity means that any artifacts that impact P_c^d will be amplified when τ is calculated, causing longer columns to give the appearance of higher τ. For example, a 1 cm water error in P_c^d in the $R = 0.95$ cm s^{-1} curve for our data (Expt. 1) would correspond to a τ error of approx. 1.2×10^4 Pa s, while the same 1 cm error in a 20 cm long column with the same Darcy velocity would correspond to a τ error of approximately 1.5×10^5 Pa s. (Numbers calculated in this way might realistically be considered to be an indication of the order of magnitude of the uncertainty in any measured τ value for a column of a given length and rate of saturation change.)

3.5. Magnitude of τ

[50] Considering the magnitudes of τ values in Figures 7, 9, and 11 of this paper, it is clear that the *uncorrected* values vary significantly between the different systems, with values as high as approximately 10^5 Pa s. However, the uncorrected values also differ considerably between sensors where multiple sensors are used—a result that itself suggests the presence of measurement artifacts.

[51] When the τ values in Figures 7, 9, and 11 are corrected to account for sensor response and pressure drop in flowing gas, the result is considerably different. If we focus on the corrected τ values (i.e., τ^*) corresponding to the fastest sensors for each set of experimental conditions (i.e., the cases where the magnitude of correction for sensor response is the least), the measured τ^* values are very small, on the order of 10^3 Pa s or less. Even considering the τ^* values from the slower sensors, it would be difficult to say conclusively from these data that τ^* is nonzero for any of the three systems studied. Furthermore, no trends are apparent between the three (very different) systems.

[52] To put the magnitude of our measured τ^* values into context, note that they are 2 to 4 orders of magnitude lower than nearly all of the recently published experimental values determined in larger columns (typically 10^5–10^7 Pa s). While some of this difference may result from uncorrected artifacts in some of the published data, it is also probable that there are some additional scale-related issues

contributing to the different results. Note that although our soil cell is smaller than the columns used in most published dynamic experiments, it is absolutely large enough to contain a representative elementary volume (REV). The length of the cell, its shortest dimension, is more than 1000× the mean diameter of the F-95 sand grains, and more than 250× the mean diameter of the SI-BG05 glass beads, factors that are orders of magnitude larger than the thresholds suggested by the microtomography work of *Costanza-Robinson et al.* [2011] for an REV. If there is a fundamental relationship between P_c^d and $\frac{\partial S}{\partial t}$, it should be measurable at this scale.

[53] Both *Camps-Roach et al.* [2010] (gas/liquid) and *Bottero et al.* [2011] (liquid/liquid) considered the effects of upscaling point measurements on the magnitude of τ, with *Camps-Roach et al.* [2010] observing negligible scale effects, and *Bottero et al.* [2011] observing an order of magnitude increase in τ with increasing scale. The difference between these results is very likely the result of the difference in the relationship between $\frac{\partial S}{\partial t}$ and $\frac{\partial S}{\partial t}\big|_{\text{avg}}$ for unsaturated versus liquid/liquid systems, as described in Sec. 3.4. While the data of *Camps-Roach et al.* [2010] show almost no difference between the local and average values, the data of *Bottero et al.* [2011] show a local $\frac{\partial S}{\partial t}$ that is an order of magnitude greater than $\frac{\partial S}{\partial t}\big|_{\text{avg}}$. Consequently, the scale effect that *Bottero et al.* [2011] observe is mathematically the result of averaging over much more nonuniform saturation field than exists in the gas/liquid experiments of *Camps-Roach et al.* [2010].

[54] Still, interestingly, even the point τ measurements of both *Camps-Roach et al.* [2010] and *Bottero et al.* [2011] are two orders of magnitude greater than the measurements reported in this work, despite the similar sensor size (*Bottero et al.* [2011] report the scale of their point measurements as 0.7 cm). One possible reason for this is that there may be a spatial mismatch in sensor response that is truncated in a smaller soil cell used here. (That is, the different fluid-selective pressure sensors may actually detect pressure in different spatial regions above or below the moving front, simply because of the need for flow to sensors to create sensor response.) Alternately, it may be that the dynamic capillary effect that creates an observed relationship between P_c^d and $\frac{\partial S}{\partial t}$ is not a homogeneous continuum phenomenon at all, but rather is caused by microheterogeneities in packing that have an impact on flow and pressure gradients that are only apparent at a larger scale [e.g., *Oliviera et al.*, 1996]. Additional work exploring these factors is needed to fully understand and predict dynamic capillary effects in porous media.

4. Conclusions

[55] Results of this work show that experimental artifacts can have a profound impact on measurement of the dynamic capillary coefficient τ, causing measured values to appear orders of magnitude greater than true values. Artifacts can also superimpose trends with saturation and system properties. The nature and magnitude of errors introduced by experimental artifacts are both system and scale dependent. When corrected for sensor response and gas pressure gradients, τ values measured in this work were found to be very small in magnitude, and largely independent of system properties. In contrast, uncorrected values were orders of magnitude larger, differed considerably between systems, and exhibited trends with saturation. Because of the small size of the experimental system used, the results of this work suggest that the dependence of measured capillary pressure on rate of saturation change may be less significant than previously thought at the REV scale.

[56] **Acknowledgement.** This material is based upon work supported by the National Science Foundation under grant 0911139.

References

Barenblatt, G. I., T. W. Patzek, and D. B. Silin (2003), The mathematical model of nonequilibrium effects in water-oil displacement, *SPE J.*, *8*(4), 409–416.

Bear, J. (1972), *Dynamics of Fluids in Porous Media*, xvii, 764 pp., American Elsevier, New York.

Bottero, S., S. M. Hassanizadeh, P. J. Kleingeld, and T. J. Heimovaara (2011), Nonequilibrium capillarity effects in two-phase flow through porous media at different scales, *Water Resour. Res.*, *47*, W10505, doi:10.1029/2011WR010887.

Bourgeat, A., and M. Panfilov (1998), Effective two-phase flow through highly heterogeneous porous media: Capillary nonequilibrium effects, *Comput. Geosci.*, *2*(3), 191–215.

Brooks, R. H., and A. T. Corey (1966), Properties of porous media affecting fluid flow, *J. Irrig. Drain. Div.*, *92*(2), 61–90.

Camps-Roach, G., D. M. O'Carroll, T. A. Newson, T. Sakaki, and T. H. Illangasekare (2010), Experimental investigation of dynamic effects in capillary pressure: Grain size dependency and upscaling, *Water Resour. Res.*, *46*, W08544, doi:10.1029/2009WR008881.

Chen, L., and T. C. G. Kibbey (2006), Measurement of air-water interfacial area for multiple hysteretic drainage curves in an unsaturated fine sand, *Langmuir*, *22*(16), 6874–6880, doi:10.1021/La053521e.

Chen, L., G. A. Miller, and T. C. G. Kibbey (2007), Rapid pseudo-static measurement of hysteretic capillary pressure-saturation relationships in unconsolidated porous media, *Geotech. Test. J.*, *30*(6), 474–483.

Costanza-Robinson, M. S., B. D. Estabrook, and D. F. Fouhey (2011), Representative elementary volume estimation for porosity, moisture saturation, and air-water interfacial areas in unsaturated porous media: Data quality implications, *Water Resour. Res.*, *47*, W07513, doi:10.1029/2010WR009655.

Dahle, H. K., M. A. Celia, and S. M. Hassanizadeh (2005), Bundle-of-tubes model for calculating dynamic effects in the capillary-pressure-saturation relationship, *Transp. Porous Med.*, *58*(1–2), 5–22, doi:10.1007/s11242-004-5466-4.

Dane, J. H., and J. W. Hopmans (2002), Water retention and storage: Laboratory, in *Methods of Soil Analysis*, edited by J. H. Dane and G. C. Topp, pp. 675–720, Soil Science Society of America, Madison, WI.

Das, D. B., and Mirzaei, M. (2012), Dynamic effects on capillary pressure relationships for two-phase flow in porous media: Experiments and numerical analyses, *AIChE J.*, doi:10.1002/aic.13777, in press.

Fischer, U., O. Dury, H. Fluhler, and M. T. vanGenuchten (1997), Modeling nonwetting-phase relative permeability accounting for a discontinuous nonwetting phase, *Soil Sci. Soc. Am. J.*, *61*(5), 1348–1354.

Friedman, S. P. (1999), Dynamic contact angle explanation of flow rate-dependent saturation-pressure relationships during transient liquid flow in unsaturated porous media, *J. Adhes. Sci. Technol.*, *13*(12), 1495–1518.

Gielen, T. W. J., S. M. Hassanizadeh, A. Leijnse, and H. F. Nordhaug (2005), Dynamic effects in multiphase flow: a pore-scale network approach, in *Upscaling Multiphase Flow in Porous Media*, edited by D. B. Das and. S. M. Hassanizadeh, pp. 217–236, Springer, Dordrecht.

Goel, G., and D. M. O'Carroll (2011), Experimental investigation of nonequilibrium capillarity effects: Fluid viscosity effects, *Water Resour. Res.*, *47*, W09507, doi:10.1029/2010WR009861.

Hassanizadeh, S. M., and W. G. Gray (1990), Mechanics and thermodynamics of multiphase flow in porous-media including interphase boundaries, *Adv. Water Resour.*, *13*(4), 169–186.

Hassanizadeh, S. M., and W. G. Gray (1993a), Toward an improved description of the physics of 2-phase flow, *Adv. Water Resour.*, *16*(1), 53–67.

Hassanizadeh, S. M., and W. G. Gray (1993b), Thermodynamic basis of capillary-pressure in porous-media, *Water Resour. Res.*, *29*(10), 3389–3405.

Hassanizadeh, S. M., M. A. Celia, and H. K. Dahle (2002), Dynamic effect in the capillary pressure-saturation relationship and its impacts on unsaturated flow, *Vadose Zone J.*, *1*(1), 38–57.

Huyakorn, P. S., and G. F. Pinder (1986), *Computational Methods in Subsurface Flow*, Academic, New York.

Kalaydjian, F. (1992), Dynamic capillary pressure curve for water/oil displacement in porous media: Theory vs. experiment, *Rep. 24813-MS*, 16 pp, Society of Petroleum Engineers, Richardson, TX.

Klute, A., and W. R. Gardner (1962), Tensiometer response time, *Soil Sci.*, *93*, 204–207.

Manthey, S., S. M. Hassanizadeh, and R. Helmig (2005), Macro-scale dynamic effects in homogeneous and heterogeneous porous media, *Transport Porous Med.*, *58*(1–2), 121–145, doi:10.1007/s11242-004-5472-6.

Muraleetharan, K. K., and C. F. Wei (1999), Dynamic behaviour of unsaturated porous media: Governing equations using the theory of mixtures with interfaces (TMI), *Int. J. Numer. Anal. Met.*, *23*(13), 1579–1608.

O'Carroll, D. M., T. J. Phelan, and L. M. Abriola (2005), Exploring dynamic effects in capillary pressure in multistep outflow experiments, *Water Resour. Res.*, *41*(11), W11419, doi:10.1029/2005WR004010.

Oliviera, I. B., A. H. Demond, and A. Salehzadeh (1996), Packing of sands for the production of homogeneous porous media, *Soil Sci. Soc. Am. J.*, *60*(1), 49–53, doi:10.2136/sssaj1996.03615995006000010010x.

Oung, O., S. M. Hassanizadeh, and A. Bezuijen (2005), Two-phase flow experiments in a geocentrifuge and the significance of dynamic capillary pressure effect, *J. Porous Med.*, *8*(3), 247–257.

Richards, L. A. (1949), Methods of measuring soil moisture tension, *Soil Sci.*, *68*(1), 95–112.

Sakaki, T., D. M. O'Carroll, and T. H. Illangasekare (2010), Direct quantification of dynamic effects in capillary pressure for drainage-wetting cycles, *Vadose Zone J.*, *9*(2), 424–437, doi:10.2136/Vzj2009.0105.

Selker, J., P. Leclerq, J. Y. Parlange, and T. Steenhuis (1992), Fingered flow in 2 dimensions. 1. Measurement of matric potential, *Water Resour. Res.*, *28*(9), 2513–2521.

Smiles, D. E., G. Vachaud, and M. Vauclin (1971), A test of uniqueness of soil moisture characteristic during transient nonhysteretic flow of water in a rigid soil, *Soil Sci. Soc. Am. Pro.*, *35*(4), 534–539.

Stauffer, F. (1978), *Time dependence of the relations between capillary pressure, water content and conductivity during drainage of porous media*, International IAHR Symposium on Scale Effects in Porous Media, Thessaloniki, Greece.

Topp, G. C., A. Klute, and D. B. Peters (1967), Comparison of water content-pressure head data obtained by equilibrium steady-state and unsteady-state methods, *Soil Sci. Soc. Am. Pro.*, *31*(3), 312–314.

Towner, G. D. (1980), Theory of time response of tensiometers, *J. Soil Sci.*, *31*(4), 607–621.

Vachaud, G., M. Vauclin, and M. Wakil (1972), Study of uniqueness of soil-moisture characteristic during desorption by vertical drainage, *Soil Sci. Soc. Am. Pro.*, *36*(3), 531.

Weitz, D. A., J. P. Stokes, R. C. Ball, and A. P. Kushnick (1987), Dynamic capillary pressure in porous media: Origin of the viscous-fingering length scale, *Phys. Rev. Lett.*, *59*(26), 2967–2970.

Wildenschild, D., J. W. Hopmans, and J. Simunek (2001), Flow rate dependence of soil hydraulic characteristics, *Soil Sci. Soc. Am. J.*, *65*(1), 35–48.

Wildenschild, D., J. W. Hopmans, M. L. Rivers, and A. J. R. Kent (2005), Quantitative analysis of flow processes in a sand using synchrotron-based x-ray microtomography, *Vadose Zone J.*, *4*(1), 112–126.